PHYSICAL REVIEW C VOLUME 24, NUMBER 1 JULY 1981

Charge and transition densities for the samarium isotopes by electron scattering

M. A. Moinester, J. Alster, and G. Azuelos*
Tel Aviv University, Ramat Aviv, Israel

J. B. Bellicard, B. Frois, M. Huet, P. Leconte, and Phan Xuan Ho
Centre d'Etudes Nucléaires de Saclay, 91190 Gif-sur-Yvette, France

(Received 1 August 1980)

We analyzed 251.5 and 401.4 MeV electron scattering data on ^{144,148,150,152}Sm. The momentum transfer ranged from 0.6 to 2.5 fm^{-1}. These isotopes span the transition region from the spherical ^{144}Sm to the deformed ^{152}Sm. Ground state charge distributions and lowest 2^+ state transition charge densities were determined via a phase shift analysis for elastic scattering and distorted-wave Born approximation calculations for inelastic scattering. Our analysis used charge densities described as a sum of spherical Bessel functions over a radius interval from zero to a cutoff of R, with densities zero at larger radii. The fitting for the ground and 2^+ states included constraints in the form of measured Barrett moments from muonic experiments and measured $B(E2)$ transition rates from muonic and other experiments. Error bands were determined for the densities including statistical and normalization uncertainties, and model dependent uncertainties associated with contributions from higher terms in the spherical Bessel function form. We find that as neutrons are added from isotope to isotope, the charge is displaced from the region of 4.0 fm to the region of 7.5 fm. The rms radii of ^{144,148,150,152}Sm were deduced with uncertainties of about 0.006 to 0.009 fm.

[NUCLEAR REACTIONS ^{144,148,150,152}Sm(e, e') analysis. Determination of charge and transition densities via Fourier-Bessel analysis.]

I. INTRODUCTION

The electromagnetic interaction has long been recognized as one of the best tools for studying nuclear structure effects. Coulomb excitation with heavy ions is used to determine transition probabilities. Muonic x-ray energies determine nuclear charge moments and electron scattering data can produce nuclear charge distributions and transition charges. The first two methods mentioned above have been in use for a long time for the study of deformed heavy nuclei. The electron scattering on those nuclei had to wait for the unique combination of high energy electron accelerators and good energy resolution capability. Our paper deals with a phenomenological analysis of electron scattering data at 251.5 and 401.4 MeV.

The even-even Sm isotopes form one of the most attractive regions for the study of nuclear deformations. Much information has been gathered over the years from heavy-ion studies. We know that the Sm nuclei span a transitional region from the almost spherical nucleus ^{144}Sm to the strongly deformed nucleus ^{154}Sm. This prior knowledge was an important asset in undertaking a systematic study of electron scattering which probes more detailed shapes of the charge densities. The capability of electrons of varying the momentum transfer, while the energy remains fixed, is essential for obtaining detailed structure information on the nuclear interior. The relevant previous studies of the Sm isotopes include heavy ion scattering below the Coulomb barrier. The results were summarized in the papers given in Ref. 1. The scattering of α's and ^{3}He above the Coulomb barrier were used to obtain the matter distributions of the Sm isotopes.[2] Hendrie[3] showed that it was necessary to treat the elastic and inelastic scattering in a coupled channel calculation. This is due to the fact that the levels in the rotational bands are strongly coupled and, due to the strong interaction of the projectile, multiple excitations are prevalent. Low momentum transfer electron scattering was done by Cardman *et al.*[4] and by Bertozzi *et al.*[5]

Recently, muonic x-ray data for the Sm isotopes have become available.[6,7] These very accurate data can be used to restrict the number of free parameters in the description of the charge densities. Bertozzi *et al.*[5] measured the electron scattering on ^{152}Sm for momentum transfers from 0.3 to 1.2 fm^{-1}. The data were analyzed in a parametrized deformed Fermi model for the intrinsic charge distribution. We previously compared their deformation parameters with those obtained from a similar analysis of our data for this nucleus. These results appeared in an earlier publication.[8] Recently, Hofmann *et al.*[9] studied the ground state rotational bands of ^{152}Sm and ^{154}Sm.

We base our analysis on elastic scattering angular distributions[8,11] for ^{144}Sm, ^{148}Sm, and ^{150}Sm in the momentum transfer range of 0.6–2.5 fm^{-1},

the inelastic scattering angular distributions to the 2^+ states in ^{148}Sm and ^{150}Sm in the same q range, and the angular distributions to the rotational band (0^+, 2^+, 4^+, and 6^+ states) in ^{152}Sm in the range of 0.6 to 2.1 fm^{-1}. The charge and transition charge densities of all the isotopes were obtained from an expansion in terms of sums of spherical Bessel functions. For all the charge distribution analyses, recent measurements[6,7] of muonic Barrett moments were used as constraints. For the 2^+ transition densities, the $B(E2)$ values from muonic and other experiments served the same purpose. Cardman *et al.*[10] used the ^{152}Sm data[8] in their evaluation of dispersive effects calculated in a coupled channel formalism which takes into account the virtual excitation of intermediate states.

II. CHARGE AND TRANSITION CHARGE DENSITIES

The elastic scattering cross sections[11] and muonic Barrett moments[12] were fitted with a phase shift analysis calculation in which the Dirac equation was solved numerically. Various "model independent" charge distribution parametrizations exist in the literature. The "sum of Gaussians" technique[13] has been used in many cases. An expansion of the charge distribution in terms of Laguerre polynomials for ^{12}C data is reported to give good fits.[14] However, the sum of spherical Bessel functions, the Fourier-Bessel analysis (FBA), has been studied the most[15–17]; we have chosen this parametrization for the extraction of densities.

The Coulomb potential is generated from the ground state charge distribution, parametrized as

$$\rho_0(r)=\begin{cases}\sum_{n=1}^{N} c_n j_0(q_n r), & r\leqslant R\\ 0, & r\geqslant R\,,\end{cases} \tag{1}$$

where the q_n are given by the condition $j_0(q_n R)=0$ (i.e., $q_n=n\pi/R$), N is an integer given by $N\approx q_{\max}R/\pi$, R is the radius cutoff beyond which the density is zero, the normalization is given by $Z=4\pi\int\rho_0(r)r^2dr$, and $q_{\max}$ is the largest q of the measurement. The error bands on the charge distributions are obtained from the error matrix:

$$[\Delta\rho(r)]^2=\sum_{\mu\nu}\sigma_{\mu\nu}^2\left(\frac{\partial\rho}{\partial c_\mu}\right)\left(\frac{\partial\rho}{\partial c_\nu}\right),$$

where

$$\sigma_{\mu\nu}^2=\left[\sum_i\frac{1}{[\Delta\sigma(\theta_i)]^2}\left(\frac{\partial\sigma(\theta_i)}{\partial c_\mu}\right)\left(\frac{\partial\sigma(\theta_i)}{\partial c_\nu}\right)\right]^{-1}$$

and $\Delta\sigma(\theta_i)$ are the uncertainties in the experimental cross sections at angles θ_i. For the ground state densities, the derivatives $(\partial\rho/\partial c_\mu)$ are calculated with the constraint of a normalized distribution. The error bands only represent the error on the charge densities at any given radius r, and it must be understood that there are very strong correlations in charge densities at different radii.[18]

It is important to estimate the model dependent contribution to the error band due to the truncation of the FBA densities after only N terms. This can be done by fitting the data also with FBA densities having more terms.[15,18] For such fits to converge one needs "data" (i.e., pseudodata) at momentum transfers higher than the maximum measured in the experiment. Our approach was to generate pseudodata at $q=n\pi/R$, with $n=N+1$, $N+2$, $N+3$, by estimating first the upper limits to the form factors.

We chose the upper limits by considering our form factor to be $F(q)=[(d\sigma/d\Omega)_{\text{exp}}/(d\sigma/d\Omega)_{\text{Mott}}]^{1/2}$, making an exponential extrapolation with the matching done at the crests of the high momentum part of the form factor. Such an extrapolation and other more conservative ones have been considered extensively by Dreher *et al.*[15] They have shown that the final densities and error bands are not sensitive to the extrapolation due to the fact that the various forms do not differ very much over the small range of extrapolation. The pseudodata cross sections were taken to be one-half the upper limit at the new q values, with the uncertainties equal to the cross sections. These pseudodata points then correspond to the estimate that the true data at these new q will be bounded by our exponential extrapolation with high probability. The extension of the number of terms in the FBA expansion, together with the addition of the corresponding pseudodata, has a negligible effect on the χ_{total}^2 since the pseudodata were taken with a 100% uncertainty.

The major source of systematic errors appears to be the choice of the cutoff radius R. For the present analysis, this is mainly due to the lack of low momentum-transfer data (0–0.6 fm^{-1}) which could determine the large radius part of the density. In Born approximation, the coefficient c_1 in the FBA series is determined by the data in the region of $q_1=\pi/R$ fm^{-1} ($q_1\simeq 0.3$ fm^{-1} for $R=11$ fm). As R is increased beyond 11 fm, the value of q_1 becomes progressively smaller compared to the first data point at $q\approx 0.6$ fm^{-1} and one cannot get converging fits. We approached the problem in two ways. In our first analysis, we chose the maximum value of R possible which does not give negative densities at large radii. When and if the

density becomes slightly nonmonotonic, the error bars are sufficiently large as to make the density consistent with a monotonic behavior. Our attitude was to allow R to be as large as possible in order not to arbitrarily exclude charge at large radii. This procedure produces different values of R_M for each nucleus. The values R_M for ^{144,148,150,152}Sm were found to be 11.0, 9.25, 10.25, and 11.0 fm, respectively. Note that the different R_M do not imply different sizes for the nuclei. In Fig. 1 are shown the normalized ground state charge distributions for ^{144,148,150,152}Sm. The error bands were obtained from the errors in the fitted parameters c_n with the constraint that the overall charge distribution be normalized—with consideration for the very significant correlations between the parameters, as obtained from the error matrix in the fitting procedure. In order to present a more sensitive display of the error band, we show in Fig. 2 the quantity $\delta\rho/\rho = \frac{1}{2}(\rho_{max} - \rho_{min})/\rho$ for ^{150}Sm.

In our second analysis, we determined best fit FBA densities for a common minimum cutoff value $R(R_L = 9.25$ fm) lower than the R_M maximum value for each isotope. The difference in the densities obtained by the two methods for ^{150}Sm are given in Fig. 2, where $\chi_{total}{}^2(R_L) = \chi_{total}{}^2(R_M) + 2.7$. The difference in these densities are larger than standard deviations, and can be considered upper limits to the error due to the R ambiguity. We note that the differences are large in regions of low and high charge radius. This means that these extreme regions are less reliably determined than the middle region. Similar checks were carried out for ^{144}Sm and ^{152}Sm. For ^{144}Sm, the $R_L - R_M$ densities differed considerably ($\approx$10% at $r = 0$) without any significant change in χ^2. We did not perform analyses with $R > R_M$, which would better define the χ^2 curve. Such analyses, allowing negative charge at high radius, would tend to raise densities at lower radii in order to preserve the overall normalization. In conclusion, we suggest that the $\rho_0(r)$ distributions analyzed with R_M are the ones that should be compared with theories, such as Hartree-Fock calculations. On the other hand, the analysis with a common R is better for the extractions of density differences between the nuclei. This becomes quite obvious for $r > R_L$ where the density differences are arbitrary.

Other systematic uncertainties in the error band

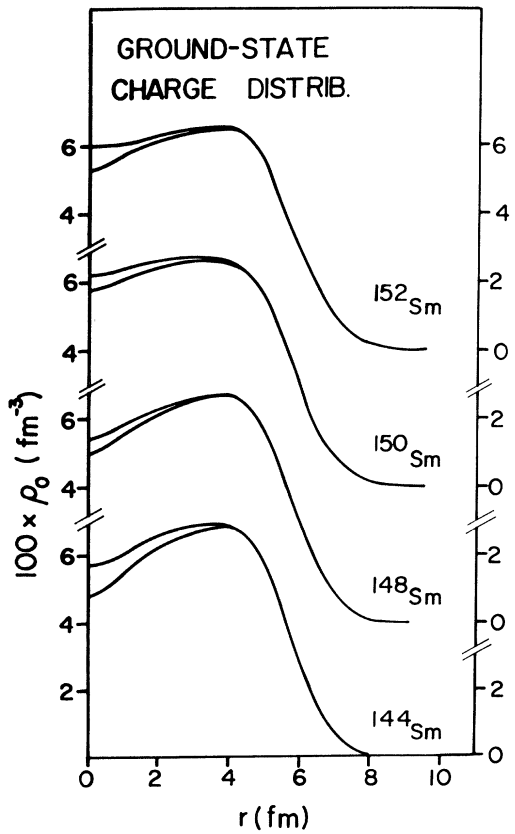

FIG. 1. The ground state charge distributions and error bands for ^{144}Sm, ^{148}Sm, ^{150}Sm, and ^{152}Sm, obtained by the Fourier-Bessel analysis, and $R = R_M$.

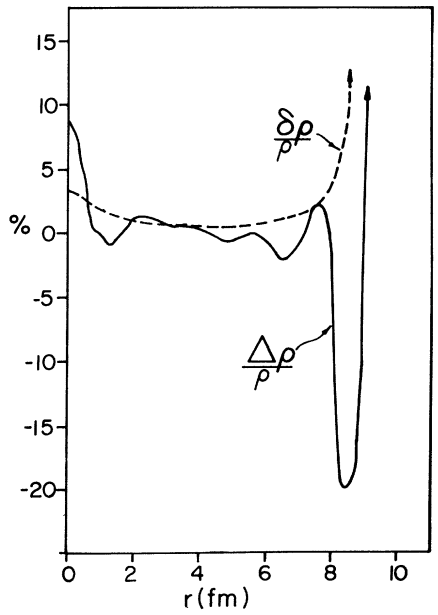

FIG. 2. The dashed curve is the relative error band $\delta\rho/\rho = \frac{1}{2}(\rho_{max} - \rho_{min})/\rho$ vs r for ^{150}Sm, in percent. The full curve is the relative change in $\rho(r)$ for cutoff radii $R_M = 10.25$ fm and $R_L = 9.25$ fm: $\Delta\rho/\rho = [\rho(r, R_M) - \rho(r, R_L)]/\rho(r, R_M)$. (See text.)

were considered by Dreher.[19] These include the effects which depend on the energy calibration and the uncertainty in the scattering angle. These effects, considered in the mentioned paper for the Mo isotopes, were found to contribute mainly at small radii. We expect that in the case of Sm the effects will be similar.

We will discuss now, in some detail, the constraints imposed by muonic x-ray data. In those studies, the energy shifts can be interpreted directly[6,7] to determine the so called Barrett[12] moments (M_B) of the charge distribution, defined as

$$\langle r^k e^{-\alpha r}\rangle = M_B(k,\alpha) = \frac{\int \rho(r) r^{k+2} e^{-\alpha r} dr}{\int \rho(r) r^2 dr} . \qquad (2)$$

The experimental uncertainties in these moments typically are very small (≈0.03%), but the major uncertainty (≈0.08%) is actually due to the large theoretical uncertainty in the calculation of the nuclear polarization (NP) contribution to the x-ray shifts.[20] We took a 40% uncertainty in the calculated NP shift for each level, and added the uncertainties for pairs of levels in quadrature. This uncertainty was then added in quadrature to the experimental uncertainties. The M_B used in our analysis are from the experiments of Powers *et al.*[6] and Yamazaki *et al.*[7] and are shown in Table I. The 40% NP error is a systematic error, and is important in the determination of absolute charge densities for a given isotope. However, for isotopic density differences a large part of the NP error would cancel. Thus our error bands, including the 40% NP error, are really upper limits when density differences are considered.

TABLE I. (a) The Barrett moments $\langle r^k e^{-\alpha r}\rangle$ used as constraints in the elastic scattering analysis. (b) The $B(E2)$ values used as constraints in the analysis of the 2_1^+ inelastic scattering.

	(a) Barrett moments (M_B)			
	α	k	M_B	Ref.
^{144}Sm	0.1246	2.2771	19.710 ± 0.013	6
^{148}Sm	0.1246	2.2771	20.057 ± 0.013	6
^{150}Sm	0.125	1.5118	5.728 ± 0.005	7
	0.125	2.2206	18.390 ± 0.011	7
	0.1246	2.2271	20.263 ± 0.013	6
	0.125	3.5482	179.79 ± 0.74	7
^{152}Sm	0.125	1.5173	5.814 ± 0.005	7
	0.125	2.2245	18.757 ± 0.012	7
	0.1246	2.2271	20.546 ± 0.013	6
	0.125	3.5534	186.33 ± 0.60	7

	(b) Constraint value (e^2fm^4)	Ref.
^{144}Sm	(3.00 ± 0.70) × 10^3	22
^{148}Sm	(7.00 ± 0.70) × 10^3	23
^{150}Sm	(1.33 ± 0.03) × 10^4	7,24
^{152}Sm	(3.44 ± 0.01) × 10^4	6,7,25

The M_B constraints were applied by including them as data points in the fitting procedure. There are several M_B values for a given isotope and they are not all independent. Only some of the available M_B were used as constraints. We chose the M_B values determined with the smallest experimental error bars and also covering the largest range of k values, not taking more than one M_B for a given k range, except for ^{150,152}Sm, where the $k \approx 2.2$ moment was available from both Refs. 6 and 7. The final results did not depend significantly on the specific choice of moments. For ^{150,152}Sm, four M_B values were used in the fitting, while for ^{144,148}Sm only one M_B was available. The best fit parameters, with the resulting rms radius values, χ_{total}^2, the number of data points (including the extra terms which were determined by the inclusion of pseudodata), and the cutoff radii are shown in Table II. The densities, shown in Fig. 1, are calculated from the best fit parameters (shown in Table II). The model dependence increases the error band by 40 to 10% for the region 0–4 fm, respectively, and is negligible at larger radii. The isotopic differences in the ground state charge distributions are shown in Fig. 3. The densities were calculated with the common $R = R_L = 9.25$ fm. The fit parameters are given in Table III. We see that with the addition of pairs of neutrons, the charge migrates from the region around 4 fm to the region of 7.5 fm. This result is similar to the observation by Dreher[19] for the Mo isotopes. The density differences given in Fig. 3 have been interpreted in terms of the interacting boson model, as described in Ref. 21.

The rms radii were calculated previously[7] using a Fermi form, whereas in our calculations they were calculated in a more model independent way. The uncertainties in the rms values (due to the Δc_n uncertainties) are reduced from about 0.0035 to 0.003 fm when the Barrett moments are included. The equivalent reduction in the density uncertainty at different radii is a factor of 2 to 3. For ^{150}Sm, the R_L density gave an $\langle r^2\rangle^{1/2}$ value about 0.004 fm smaller than the R_M density. Considering the R variation as well as the Δc_n variation, we estimate total uncertainties of about ±0.006 fm for ^{148,150,152}Sm and ±0.009 fm for ^{144}Sm. For ^{152}Sm our rms result is larger than that of Cardman *et al.*[10] for the same electron scattering data. However, their analysis did not include the Barrett moments.

TABLE II. Best fit parameters for FBA from combined analysis of muonic and elastic scattering data. The values C_i are the coefficients in Eq. (1); R is the cutoff radius for the fit, χ_{total}^2 is the total χ^2 value of the best fit; the number of data points includes the pseudo-data and the Barrett moments. $\langle r^2\rangle^{1/2}$ are the values obtained from the fit and systematic errors are included.

	^{144}Sm	^{148}Sm	^{150}Sm	^{152}Sm
C_1	0.051 75	0.073 85	0.059 61	0.050 73
C_2	0.055 98	0.024 02	0.044 98	0.051 25
C_3	−0.035 18	−0.059 43	−0.043 81	−0.032 77
C_4	−0.038 69	0.010 76	−0.015 80	−0.030 82
C_5	0.019 63	0.017 02	0.022 58	0.017 16
C_6	0.014 28	−0.011 40	0.000 85	0.011 49
C_7	−0.009 71	−0.001 81	−0.007 98	−0.004 98
C_8	−0.006 21	0.000 93	−0.000 75	−0.006 42
C_9	0.001 38	0.000 98	0.001 15	0.001 00
C_{10}	0.000 15	−0.001 26	0.000 25[a]	0.000 04
C_{11}	0.000 90[a]	−0.001 74[a]	−0.000 77[a]	0.000 40[a]
C_{12}	−0.001 18[a]			
R (fm)	11.0	9.25	10.25	11.0
χ_{total}^2	11.8	15.1	9.5	10.3
Number of data points	24	27	30	27
$\langle r^2\rangle^{1/2}$ (fm)	4.947 ± 0.009	5.002 ± 0.006	5.045 ± 0.006	5.093 ± 0.006

[a] These parameters were fitted but were kept fixed in the last iteration.

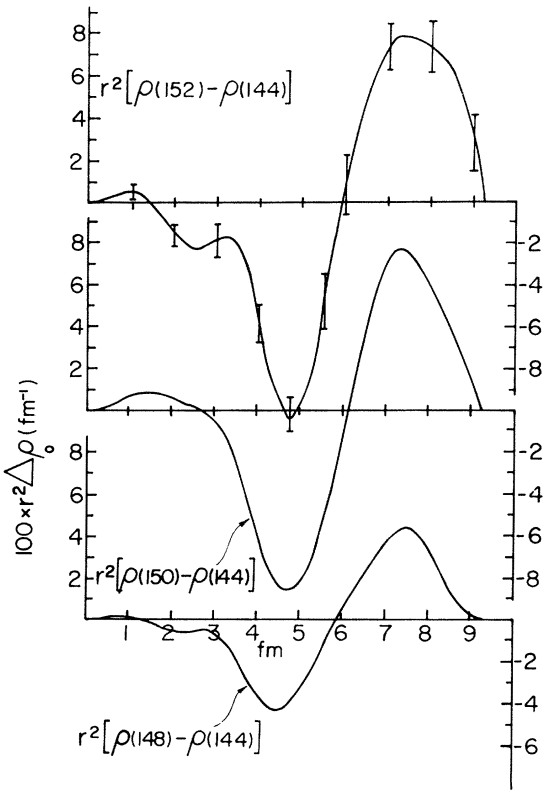

FIG. 3. The differences between the charge densities multiplied by r^2. The fits use the common $R = R_L = 9.25$ fm. The errors shown for some values of r are determined by adding the individual errors in quadrature.

The inelastic cross section data to the 2_1^+ states of ^{144,148,150,152}Sm were fitted in distorted-wave Born approximation (DWBA) analysis with a parametrization similar to that for the ground state. The best fit ground state charge distributions of

TABLE III. Best fit parameters for FBA from combined analysis of muonic and elastic scattering data. The values C_i are the coefficients in Eq. (1). The cutoff is $R = 9.25$ fm. χ_{total}^2 is the total χ^2 value of the best fit. The number of data points includes the pseudo-data and the Barrett moments. The ^{148}Sm coefficients are the same as in Table II.

	^{144}Sm	^{150}Sm	^{152}Sm
C_1	0.074 72	0.073 32	0.072 63
C_2	0.026 14	0.024 62	0.021 82
C_3	−0.063 82	−0.052 76	−0.054 10
C_4	0.010 43	0.010 58	0.009 83
C_5	0.019 18	0.015 35	0.016 21
C_6	−0.012 57	−0.009 56	−0.006 56
C_7	−0.003 97	−0.001 88	0.005 36
C_8	−0.001 87	−0.000 79	−0.001 41
C_9	0.001 26	0.001 01	−0.000 99
C_{10}	−0.001 19	−0.002 66	−0.002 30
C_{11}	−0.001 57[a]	−0.001 83[a]	
χ_{total}^2	11.5	12.2	24.0
Number of data points	24	30	27

[a] These parameters were fitted but were kept fixed in the last iteration.

Eq. (2) were used to calculate the distortion of the incoming and outgoing waves. Here the transition charge densities are expanded as

$$\rho_2(r)=\begin{cases}\sum_{n=1}^{N} c_n j_2(q_n r), & r \leq R\\ 0, & r \geq R\,,\end{cases} \tag{3}$$

and the q_n are given by the condition $j_2(q_n R)=0$, with a common radius cutoff $R=11$ fm. The cutoff was chosen at the high side of the values found in elastic scattering since it is known that the transition radius is larger than the rms radius. Simultaneous fits for the data at both energies were done with constraints on $B(E2)$ values. The constraining $B(E2)$ values are given in Table I and were introduced as extra data in the fits. The best fit parameters are shown in Table IV, together with the values of χ^2_{total}. Also shown in the table are the values of the transition radii which are defined as

$$R^L_{\text{tr}}=\left(\int \rho_L(r) r^{L+4} dr \Big/ \int \rho_L(r) r^{L+2} dr\right)^{1/2}. \tag{4}$$

TABLE IV. Best fit parameters for FBA from analysis of 2^+_1 scattering and $B(E2)$ data. The values C_i are the coefficients in Eq. (3); χ^2_{total} is the total χ^2 value of the best fit; the number of data points includes the pseudodata and the $B(E2)$ value; R_{tr} is the transition radius defined in Eq. (4). A common $R=11.0$ fm is used.

	^{144}Sm	^{148}Sm	^{150}Sm	^{152}Sm
C_1	0.024 97	0.034 09	0.044 55	0.069 92
C_2	0.023 25	0.025 30	0.033 86	0.049 72
C_3	−0.020 72	−0.034 41	−0.046 37	−0.073 09
C_4	−0.016 36	−0.007 62	−0.018 58	−0.020 89
C_5	0.006 44	0.025 49	0.031 47	0.047 11
C_6	0.013 62	0.006 22	0.002 69	−0.001 31
C_7	−0.003 97	−0.013 81	−0.016 02	−0.023 87
C_8		−0.003 31	−0.003 97	−0.020 89
C_9		−0.007 86	0.004 27	0.006 00
C_{10}		0.003 61	0.004 73	0.007 44
C_{11}		−0.000 52[a]	0.000 86	
χ^2_{total}	6.6	20.5	23.9	7.9
No. of data	13	25	26	24
R_{tr} (fm)[b]	6.12	6.34	6.70	6.80
$B(E2)$[c] (e^2fm^4)	3.28×10^3	6.92×10^3	1.33×10^4	3.44×10^4

[a] This parameter was fitted but was kept fixed in the last iteration.

[b] The statistical error bars are approximately 0.04 fm for ^{148,150,152}Sm. The total error, including systematic errors associated with the choice of R, is significantly larger.

[c] These values are determined mainly by the $B(E2)$ constraints of Table I and are not the values associated with the (e,e') experiment alone. The error bars are of the same order as for the constraint values.

The 2^+ transition charge densities may also have ambiguities related to the choice of the cutoff radii R. In this case we did not study the magnitude of these uncertainties. Parameters such as the transition charge radius, which depend on an r^6 weighting, may be sensitive to R variations and other types of model uncertainties. For example, one could have a modified FBA form where an exponential tail is matched to the density at some large radius. Such a model could alter the shapes of the resulting densities and it would be difficult to argue in favor of one form or another. Still, such an approach would take us further from model independence. One could say that the utilization of different forms can give a measure of the model sensitivities involved in using a particular form. Figure 4 shows the transition charge distributions of ^{144,148,150,152}Sm. These distributions have also been interpreted in terms of the interacting boson model. [21]

For ^{144}Sm, where the data extended only to $q=1.2$ fm^{-1}, the deduced 2^+ transition density has larger uncertainties than for the other isotopes. The limited q range allowed FBA fits, without pseudodata, with only three Bessel functions. The fits shown involved seven Bessel functions and included four pseudodata points at momentum transfers ranging up to 2.3 fm^{-1}. The addition of the four pseudodata points increased the size of the error band compared to the FBA fit with three Bessel functions, as is the case for all other fits. The shape with seven Bessel functions is similar to that determined with three Bessel functions, but whould be preferred. Still, because the number of pseudodata points was comparable to the number of real data points, the ^{144}Sm 2^+ transition density and error band should be considered less reliable than the results for the other isotopes.

III. DISPERSIVE EFFECTS

A coupled channel calculation, based upon the experimental data for ^{152}Sm, was performed by Cardman *et al.* [10] The calculations took into consideration all the allowed transitions between the lowest 0^+, 2^+, 4^+, and 6^+ states. They found that for the 0^+ and 2^+ states of ^{152}Sm, the contribution of these second order effects is at most 5% in the regions of the minima and is negligible elsewhere. Even though these dispersion corrections are not negligible in the regions of the minima, their effect on the charge density and the 2^+ transition charge density is small. A comparison of the DWBA and coupled channel analyses showed that the contribution of second order effects to the transition densities fall w' l within the experimental errors. The coupling of collective states

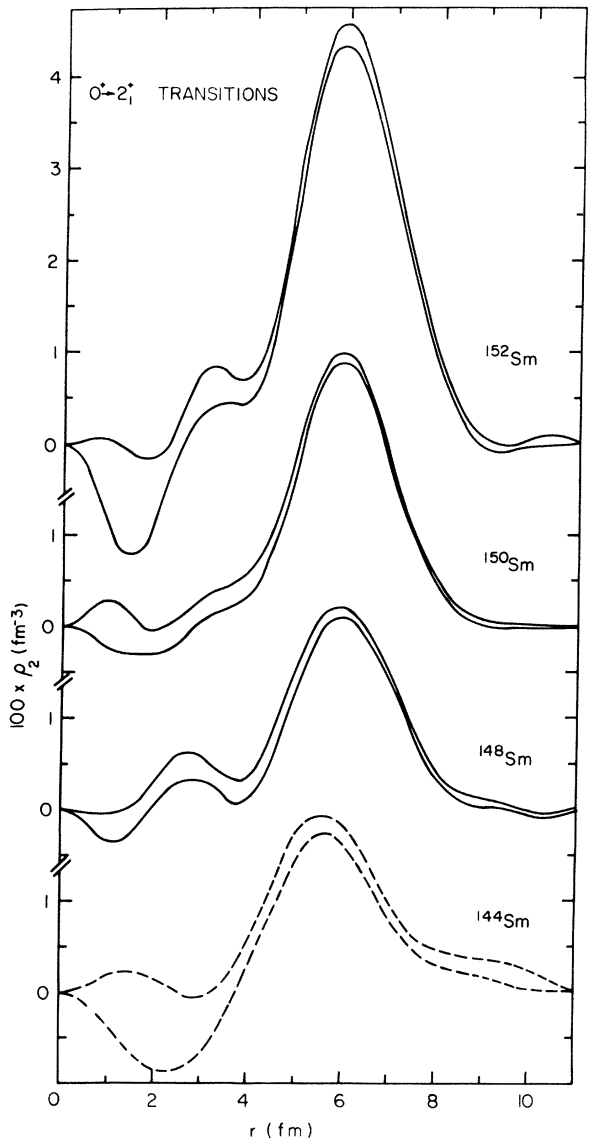

FIG. 4. The transition densities and error bands for the first excited 2^+ states in ^{144}Sm, ^{148}Sm, ^{150}Sm, and ^{152}Sm. The ^{144}Sm transition density is presented by a dashed curve to indicate the smaller reliability, as explained in the text.

in ^{144,148,150}Sm to the ground states is smaller than for ^{152}Sm. Thus second order effects in these nuclei will be even smaller than for ^{152}Sm. Hence, the use of the DWBA procedure for analyzing the experimental results is adequate for the present level of experimental accuracy.

IV. ROTATIONAL MODEL DESCRIPTION OF ^{152}Sm

A description of the ^{152}Sm results in terms of a rotational model has already been reported elsewhere.[8] In the rotational model, the intrinsic ground state charge distribution can be described by

$$\rho_{g.s.}(r,\theta)=\rho_0(r)+\sum_L \rho_L Y_{L0}(\theta)\,, \tag{6}$$

where the terms $\rho_L(r)$ are the transition charge densities for exciting the states of the ground state rotational band. The density $\rho_{g.s.}(r,\theta)$ satisfies

$$Z=\int\rho_{g.s.}(r,\theta)d\Omega=4\pi\int\rho_0 r^2 dr \tag{7}$$

and

$$\rho_L(r)=2\pi\int\rho_{g.s.}(r,\theta)Y_{L0}\sin\theta\, d\theta \quad (L\neq 0) \tag{8}$$

with

$$B(EL)_t=\left|\int\rho_{g.s.}(r,\theta)r^2 Y_{L0}d\Omega\right|^2 = \left|\int\rho_L(r)r^{L+2}dr\right|^2 . \tag{9}$$

In previous work, we assumed a deformed Fermi shape for $\rho_{g.s.}(r,\theta)$. In the present analysis, no initial shape was assumed for the intrinsic distribution. We determined ρ_0 and ρ_2 for the 0^+ and 2^+ states of ^{152}Sm. The transition densities ρ_4 and ρ_6 can be determined from the FBA analysis of the 4^+ and 6^+ form factors. These form factors were reported in Ref. 8 and by Hofmann *et al.*[9], and have recently been remeasured[14] and extended also to higher momentum transfer. The transition densities ρ_4 and ρ_6 will therefore be reported at a later date. Together with ρ_0 and ρ_2 determined here, Eq. (6) will then give the deformed intrinsic ground state charge distribution. This charge distribution is limited in its correctness by the extent to which the low levels of ^{152}Sm are indeed described by a pure rotational model. The density of Eq. (6) is superior to the deformed Fermi shape in that it gives a better χ^2 fit for the 0^+, 2^+ data [$\chi_{total}=18$ for Eq. (6) compared to $\chi_{total}^2=101$ for the deformed Fermi shape].

V. SUMMARY AND CONCLUSIONS

We analyzed 251.5 and 401.4 MeV electron scattering data on ^{144,148,150,152}Sm. The momentum transfer ranged from 0.6 to 2.5 fm^{-1}. We extracted ground state charge distributions in a phase shift analysis of the elastic scattering cross sections and muonic Barrett moments. Such an analysis determines the best density that can be obtained from experimental data. Our analysis used charge densities parametrized as a sum of spherical Bessel functions over a radius interval from zero to a cutoff of R, with densities zero at larger radii. We found that the resulting densities are sensitive to the choice of the cutoff radius. We explained how the sensitivity to cut-

off radius is related to the absence of low-q data. For a given isotope, we chose for the optimum cutoff radius the largest cutoff radius possible subject to the condition that the density at large radii would not be negative.

We determined error bands for the charge distributions from the error matrix of the χ^2 fit, where these error bands depend on the statistical and normalization uncertainties in the experimental cross sections, as well as the uncertainties associated with the truncation of the Fourier-Bessel series. We discuss in detail the charge distribution uncertainties due to the cutoff radius ambiguity; generally, the uncertainties are largest for very small and very large radii. The Barrett moment constraints impose severe limitations on the choice of charge distributions, also reducing the density uncertainty at different radii by a factor of 2 to 3. We discuss in detail the dependence of the error bands on the truncation of the Fourier-Bessel series.

The rms radii of ^{144,148,150,152}Sm were deduced with uncertainties of about 0.006 to 0.009 fm. The increase in rms values is faster than $A^{1/3}$. The charge density differences show that charge migrates from the region around 4 to 7.5 fm with the addition of pairs of neutrons.

The inelastic cross section data to the 2_1^+ states of ^{144,148,150,152}Sm were fitted in a DWBA analysis with a parametrization similar to that for the ground state. We used measured $B(E2)$ values from other experiments as a constraint in the fitting determination of the transition densities. The error bands for these densities include statistical, normalization, and truncation errors, as in the ground state analysis. The 2_1^+ densities are very similar in shape for all isotopes; the main difference is in their amplitudes. There is a slight but steady increase in the transition radius between ^{144}Sm and ^{152}Sm. The results are consistent with an increase in the coupling strengths of the 2_1^+ states to the ground states in the transition from the spherical ^{144}Sm to the deformed ^{152}Sm. For ^{152}Sm, we show how to obtain the intrinsic deformed charge distribution from the charge and transition densities of the ground state band.

The densities we determined here should be compared to Hartree-Fock calculations and can also be interpreted in terms of the interacting boson model.

ACKNOWLEDGMENTS

We acknowledge useful discussions with Dr. Haik, Dr. Powers, Dr. Shera, Dr. Wohlfart, and Dr. Yamazaki. The Tel Aviv University physicists thank Dr. Tzara, Dr. Catillon, and Dr. Netter for their hospitality during their stay at the Saclay electron accelerator.

*Present address: University of Montreal, TRIUMF, Vancouver, British Columbia V6T 1W5, Canada.

[1]W. Bruckner, D. Husar, D. Pelte, K. Traxel, M. Samuel, and U. Smilansky, Nucl. Phys. A231, 159 (1974); Phys. Rev. Lett. 30, 57 (1973); T. K. Saylor, J. X. Saladin, I. Y. Lee, and K. A. Erb, Phys. Lett. 42B, 51 (1972); R. Eagle, N. M. Clarke, R. J. Griffiths, C. B. Fulmer, and D. C. Hensley, Phys. Rev. C 16, 1314 (1967).

[2]G. Palla and C. Pegel, Nucl. Phys. A231, 317 (1979) and references therein.

[3]D. L. Hendrie *et al.*, Phys. Lett. 26B, 127 (1967).

[4]L. S. Cardman, D. Kalinsky, J. Legg, R. Yen, and C. K. Bockelman, Nucl. Phys. A216, 285 (1973) and references therein.

[5]W. Bertozzi, T. Cooper, N. Ensslin, J. Heisenberg, S. Kowalski, M. Mills, W. Turchinets, and C. Williamson, Phys. Rev. Lett. 28, 1711 (1972).

[6]R. J. Powers, P. Barreau, B. Bihoreau, J. Miller, J. Morgenstern, J. Picard, and L. Roussel, Nucl. Phys. A316, 295 (1979).

[7]Y. Yamazaki, E. B. Shera, M. V. Hoehn, and R. M. Steffen, Phys. Rev. C 18, 1474 (1978); Y. Yamazaki, H. D. Wohlfahrt, E. B. Shera, and M. V. Hoehn, Phys. Rev. Lett. 22, 1470 (1979).

[8]A. Nakada, N. Haik, J. Alster, J. B. Bellicard, S. Cochavi, B. Frois, M. Huet, P. Leconte, P. Ludeau, M. A. Moinester, Phan Xuan Ho, and S. Turck, Phys. Rev. Lett. 38, 534 (1977).

[9]R. Hofmann, H. G. Anderson, B. Dreher, S. Glückert, and R. Neuhausen, in Abstracts of Contributed Papers, International Conference on Nuclear Physics with Electromagnetic Interactions, Mainz, 1979.

[10]L. S. Cardman, D. H. Powell, R. L. Gulbranson, D. G. Ravenhall, and R. L. Mercer, Phys. Rev. C 18, 1388 (1979).

[11]N. Haik, Ph.D. thesis, Tel Aviv University (1979) data tables available from authors; N. Haik *et al.* (unpublished).

[12]R. C. Barrett, Phys. Lett. 33B, 388 (1970).

[13]I. Sick, Nucl. Phys. A218, 509 (1974).

[14]L. S. Cardman, P. Leconte, D. C. Ravenhall, and S. E. Williams, in Abstracts of Contributed Papers, International Conference on Nuclear Physics with Electromagnetic Interactions, Mainz, 1979.

[15]B. Dreher, J. Friedrich, K. Herle, H. Rothhaas, and G. Luhrs, Nucl. Phys. A235, 219 (1974).

[16]H. Rothhaas *et al.*, Phys. Lett. 51B, 23 (1974).

[17]J. L. Friar and J. W. Negele, Nucl. Phys. A212, 93 (1973).

[18]J. Borysowicz and J. H. Hetherington, Phys. Rev. C 7, 2293 (1973).

[19]B. Dreher, Phys. Rev. Lett. 35, 716 (1975).

[20]G. A. Rinker and J. Speth, Nucl. Phys. A306, 360 (1978).

[21]M. A. Moinester, J. Alster, G. Azuelos, and A. E. L.

Dieperink (unpublished).
[22]T. W. Barrows and R. L. Auble, Nucl. Data Sheets 16, 231 (1975).
[23]B. Harmatz and J. R. Shepherd, Nucl. Data Sheets 20, 373 (1977).
[24]C. M. Baglin, Nucl. Data Sheets 18, 223 (1976).
[25]H. Fischer *et al.*, Phys. Rev. C 15, 921 (1977).